

UC Irvine

UC Irvine Previously Published Works

Title

Non-Invasive Monitoring of Oxygen Tension and Oxygen Transport Inside Subcutaneous Devices After H₂S Treatment.

Permalink

<https://escholarship.org/uc/item/06p3d7nh>

Authors

Najdahmadi, Avid

Smink, Alexandra

de Vos, Paul

et al.

Publication Date

2020

DOI


10.1177/0963689719893936

Copyright Information

This work is made available under the terms of a Creative Commons Attribution-NonCommercial License, available at <https://creativecommons.org/licenses/by-nc/4.0/>

Peer reviewed

Non-Invasive Monitoring of Oxygen Tension and Oxygen Transport Inside Subcutaneous Devices After H₂S Treatment

Cell Transplantation
Volume 29: 1-9
© The Author(s) 2020
Article reuse guidelines:
sagepub.com/journals-permissions
DOI: 10.1177/0963689719893936
journals.sagepub.com/home/ctj


Avid Najdahmadi¹ , Alexandra M. Smink², Paul de Vos², Jonathan R.T. Lakey^{3,4} , and Elliot Botvinick^{1,3,4}

Abstract

Medical devices for cell therapy can be improved through prevascularization. In this work we study the vascularization of a porous polymer device, previously used by our group for pancreatic islet transplantation with results indicating improved glycemic control. Oxygen partial pressure within such devices was monitored non-invasively using an optical technique. Oxygen-sensitive tubes were fabricated and placed inside devices prior to subcutaneous implantation in nude mice. We tested the hypothesis that vascularization will be enhanced by administration of the pro-angiogenic factor hydrogen sulfide (H₂S). We found that oxygen dynamics were unique to each implant and that the administration of H₂S does not result in significant changes in perfusion of the devices as compared with control. These observations suggest that vascular perfusion and density are not necessarily correlated, and that the rate of vascularization was not enhanced by the pro-angiogenic agent.

Keywords

oxygen monitoring, tissue engineering, islet transplantation, diabetes, medical devices, biophotonics

Introduction

Tissue engineering approaches to create bioartificial organs have been emerging in the past few decades^{1,2}. In the case of the pancreas, as related to endocrine function, evidence suggests that it is unnecessary to replace the whole organ. It is shown that transplantation of the islets of Langerhans that contain the endocrine cells also results in restoration of the endocrine function³. For example, transplantation of isolated pancreatic islets is used to treat type 1 diabetes (T1D). T1D is caused by autoimmune destruction of pancreatic beta cells⁴. These cells normally synthesize and secrete insulin, which is an important hormone involved in physiological regulation of blood glucose. Self-monitoring of blood glucose (by lancet blood draw and glucose meter) in conjunction with multi-daily injections of insulin is the standard of care. However, the resulting glycemic control is imperfect and can cause harmful secondary complications such as cardiovascular diseases, retinopathy, and nephropathy⁵⁻⁷. A promising alternative to daily insulin injections is transplantation of pancreatic islet cells. This transplantation can provide autonomous regulation of blood glucose concentration and therefore result in stable glycemic control, thus

preventing secondary complications⁸. Islet transplantation into the portal vein has resulted in insulin independency in the first year; however, the insulin independency was shown to decrease to less than 50% after 5 years^{9,10}. These findings support the potential for pancreatic islets to treat T1D; however, in consideration of the 5-year half life, inaccessibility for islet retrieval, and risk to the liver, better approaches are needed.

¹ Department of Materials Science and Engineering, University of California Irvine, Irvine, CA, USA

² Department of Pathology and Medical Biology, University Medical Center Groningen, University of Groningen, Groningen, the Netherlands

³ Department of Biomedical Engineering, University of California Irvine, Irvine, CA, USA

⁴ Department of Surgery, University of California Irvine, Irvine, CA, USA

Submitted: October 26, 2018. Revised: October 21, 2019. Accepted: November 8, 2019.

Corresponding Author:

Elliot Botvinick, Department of Biomedical Engineering, University of California Irvine, Irvine, CA, USA.
Email: elliott.botvinick@uci.edu



Creative Commons Non Commercial CC BY-NC: This article is distributed under the terms of the Creative Commons Attribution-NonCommercial 4.0 License (<https://creativecommons.org/licenses/by-nc/4.0/>) which permits non-commercial use, reproduction and distribution of the work without further permission provided the original work is attributed as specified on the SAGE and Open Access pages (<https://us.sagepub.com/en-us/nam/open-access-at-sage>).

Polymer devices for housing islets are being developed to improve the outcomes of islet transplantation. A variety of polymer systems as well as implantation sites have been investigated^{11–17}. Literature suggests that the subcutaneous space can be advantageous for cellular transplantation because of ease of access and less invasive surgical procedures, but because of low oxygen tension and vascularization under the skin, hypoxia can occur^{18,19}. Hypoxia can induce apoptosis and necrosis and ultimately compromise the functionality of transplanted cells²⁰. Multiple groups have shown that islet transplantation under the skin can be successful after modulation of the site with a device^{21,22}. Critical to the success of these devices is adequate supply of oxygen, which can be provided if sufficient vascular perfusion is introduced. Such perfusion can be stimulated by using microporous structures²³, inclusion of angiogenic factors²⁴, co-transplantation of vascular inductive cell types, or devices that can be implanted for prevascularization prior to transplantation of the cells²⁵. A well-vascularized device will provide reduced diffusional distances between the newly formed vasculature and the transplanted cells and result in faster transport dynamics of nutrients and oxygen, preventing the loss of cells by hypoxia. We have developed a porous poly(D, L-lactide-co- ϵ -caprolactone) (PDLLCL) polymer scaffold that has shown successful results in promoting islet-cell survival and achieving normoglycemia under the skin of athymic nude mice for the duration of a 70 day study²⁶. This porous scaffold is designed for inducing vascularization *in vivo* and can potentially compensate for loss of perfusion through the interpenetrating islet capillary network following isolation. Our previous results²⁶ suggest that further increasing the vascularization of these devices may lead to a faster return to normoglycemia with lower number of islets.

In this study, we investigated hydrogen sulfide (H_2S) as an agent to improve vascularization of the PDLLCL device. H_2S is a gaseous signaling molecule, like nitric oxide and carbon monoxide, normally produced by the body. It was first described as a neuromodulator²⁷, but was later recognized for its effects on vascular cells²⁸. Endogenous H_2S is enzymatically generated in vascular cells, where it exhibits vasoactive, anti-oxidant, anti-inflammatory, and anti-apoptotic properties²⁸. The effects of H_2S are well described, but the molecular pathways of its action are poorly understood. Cai and coworkers were the first to show that intraperitoneal injections of the exogenous H_2S donor NaHS stimulate angiogenesis in subcutaneous Matrigel plugs in mice²⁹. Increased angiogenesis was shown by higher hemoglobin levels and the presence of more capillaries with NaHS administration at concentrations of 10 and 50 $\mu\text{mol}/(\text{kg}\cdot\text{d})$ as compared with the untreated group. Here we investigate whether H_2S will have a similar effect on vascularization of our PDLLCL devices implanted into the subcutaneous compartment as assessed by histology, CD31 expression, and an optical measure of oxygen transport between vasculature and the device.

Materials and Methods

Device Preparation

Devices were obtained from Polyganics B.V. (Groningen, The Netherlands). A 4% (w/v) PDLLCL solution was prepared in chloroform (Sigma-Aldrich, Zwijndrecht, The Netherlands). The PDLLCL solution was thoroughly mixed with sodium chloride particles (Sigma-Aldrich, Zwijndrecht, The Netherlands) of 250–425 μm (10:1 w/w) in order to create a porous structure. This solution was transferred into sterile glass Petri dishes to allow the solvent to evaporate. To remove the salt particles, the polymer sheet (5 mm thick) was extensively washed with sterile H_2O . The polymer sheet was casted and resized, resulting in a 10 mm by 15 mm device. During the casting process three channels were created by introducing 400 μm diameter iron rods. These channels were created to accommodate cells, and in the current study they were used for insertion of the oxygen-sensitive tubes (OSTs) to non-invasively monitor the oxygen tension *in vivo* (Fig. 1A). The scaffolds were stored in 70% ethanol for several days to sterilize the scaffolds before implantation.

OST Fabrication

OSTs comprise an oxygen-permeable tube and an oxygen-sensitive dye. The selected oxygen-sensitive dye is platinum(II)-meso-tetra (4-fluorophenyl) tetrabenzoporphyrin (PtTPTBPF), which has peak absorptions at 430 and 614 nm and emission peak at 773 nm (Frontier Scientific, Logan, UT, USA). This dye was mixed with polystyrene (MW 2500, Sigma, St. Louis, MO, USA) and dissolved into a solution using chloroform (Sigma, St. Louis, MO, USA), to form the dye solution. The dye solution contains 4 mg PtTPTBPF, 60 mg polystyrene and 900 μL chloroform. The dye solution was flushed through an oxygen-permeable biocompatible silicone tubing (BTSIL-037, Instech Laboratories, Plymouth Meeting, PA, USA) five times to form a homogenous inner coating of PtTPTBPF inside the silicone tubes. The tubes were stored in a well-ventilated dark environment at 24°C for a duration of 24 h to allow the remaining chloroform to evaporate. A stainless steel wire (24 Gauge A1 Wire, Kanthal, Sweden) was then inserted into each tube in order to provide mechanical stability (Fig. 1B). Afterwards the tubes containing a wire were cut to a length matching the PDLLCL device (15 mm) and the ends were sealed using medical-grade silicone adhesive (MED-1000 Nusil, Carpinteria, CA, USA). The sealed tubes were kept at room air in a dark environment for 2 days to fully cure. OSTs were sterilized by immersion in 70% ethanol for 12 h.

The Oxygen Monitor

An oxygen monitor was fabricated a previously described³⁰. The monitor is placed onto the surface of skin, emits light through the skin and onto the implanted OSTs, and receives luminescence to record luminescent waveforms. The

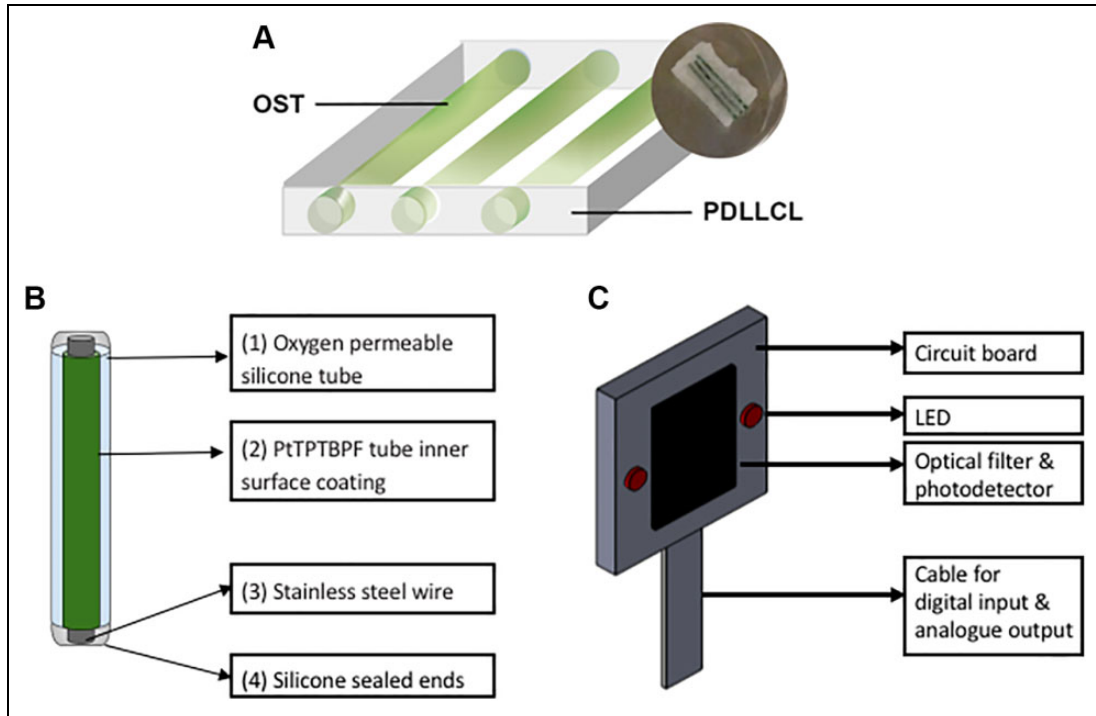


Figure 1. (A) Oxygen-sensitive tubes (OSTs) shown as green cylinders (15 mm in length) are inserted into three empty channels of the porous PDDLCL device (5 mm × 10 mm × 15 mm) to quantify oxygen tension. (B) OSTs act as retrievable oxygen-monitoring sensors and are made of oxygen-permeable silicone tubing coated on the inner surface with a layer of PtTPTBPF and reinforced with stainless steel wire. Both ends are sealed using medical-grade silicone adhesive. (C) Oxygen monitor comprising a printed circuit board that houses two LEDs, photodetector and optical filter.

monitor comprises a printed circuit board that houses a silicon photodetector bracketed by two light-emitting diodes (LEDs) having central emission wavelength of 617 nm (Fig. 1C). An optical bandpass filter is mounted onto the detector to reject the LED wavelengths while passing the dye emission wavelengths. For each oxygen measurement both LEDs flash simultaneously 25 times at 1% duty cycle (100 μs on, 10,200 μs off) to excite the oxygen-sensitive porphyrin dye. The emission of the dye after each flash is passed through an optical filter and onto the photodiode. Photodiode electrical current is converted to voltage by an operational amplifier and sampled over a period of 200 μs at a sampling frequency of 500 kHz using a myRIO data acquisition module (National Instruments, Austin, TX, USA). LED and data acquisition timing is controlled by LABVIEW 2015 (National Instruments, Austin, TX, USA). The dye continues to emit light after the end of each LED emission period with a decay that can modeled as exponential:

$$V = V_0 e^{\left(\frac{-t}{\tau}\right)}$$

where V is the detector voltage, V_0 is the voltage at the start of the decay, t is time in seconds, τ is the lifetime parameter reported in seconds. Lifetime values were computed from emission waveforms using the *fit* function in MATLAB (MathWorks, Natick, MA, USA) configured for nonlinear

least squares regression. The average τ for all 25 cycles is hereafter reported as lifetime (τ). The porphyrin dye emission is quenched by oxygen and consequently lifetime values (τ) decrease with increasing PO_2 .

OST Calibration

A custom-built glass chamber with an inlet and outlet port was placed above the oxygen monitor. OST were individually placed inside the chamber and exposed to different gases mixtures at atmospheric pressure comprising 160, 76, 38, and 0 mmHg oxygen. τ was measured at each oxygen partial pressure to generate a calibration curve (Fig. 2A). This process is repeated for each OST individually. OSTs were matched for calibration in groups of three and inserted into devices.

Implantations and NaHS Injections in Animals

The University of California Institutional Animal Care and Use Committee at the University of Irvine approved all described animal procedures (IACUC # 2008-2850). Animals were housed at the University of California Irvine animal facility and maintained under 12-hour light/dark cycles with *ad libitum* access to water and standard chow. Devices were implanted in male athymic nude mice (Foxn1^{nu}, Charles

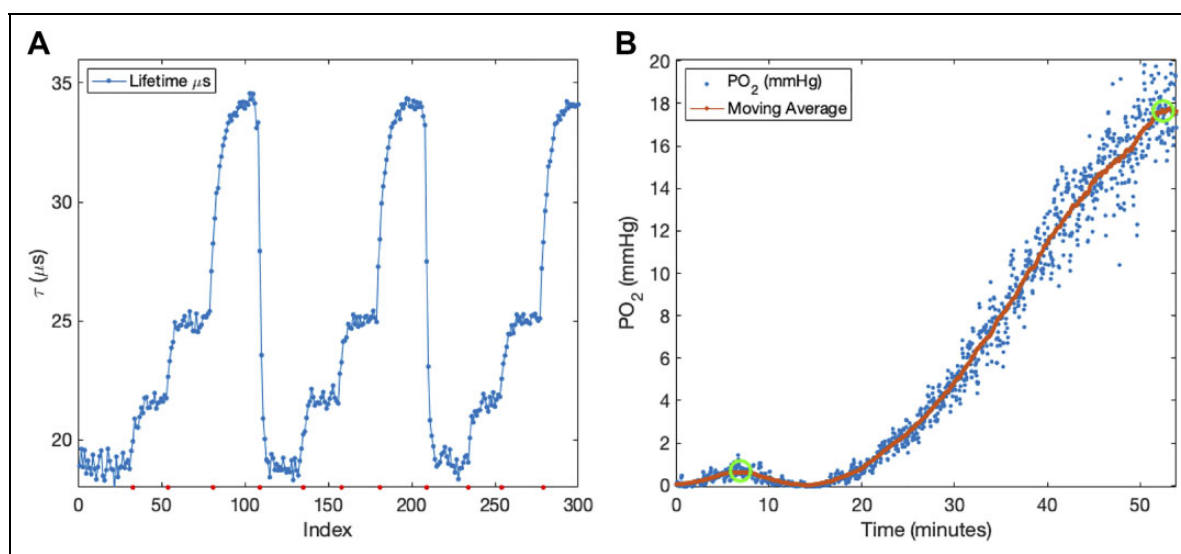


Figure 2. (A) Three calibration cycles of a single oxygen-sensitive tube (PO_2 : 160, 76, 38, and 0 mmHg, in order). Average lifetime values for each plateau (at each gas mixture) across the three cycles are 19.0 ± 0.07 , 21.6 ± 0.08 , 24.9 ± 0.04 and 34.1 ± 0.06 μ s, respectively. (B) DIGT performed on an animal 3 days after device implantation. *Risetime* is defined as elapsed time between exchanging inhaled gas from 152 to 760 mmHg (left green circle) and steady state (right green circle).

River, Wilmington, MA, USA) 8 weeks old. Briefly, under anesthesia a small incision was made in the skin to create a subcutaneous pocket on the back of the mouse. PDLCL devices containing the calibrated OSTs and fibrin were placed into this pocket and the skin was closed using skin staples (Cellpoint Scientific, Gaithersburg, MD, USA). All mice received ibuprofen water (0.2 mg/mL; Banner Pharmacaps, High Point, NC, USA) as analgesic post-surgery for 2 days. Since H_2S is a gas, we used a sodium hydrosulfide (NaHS) solution as a H_2S donor. NaHS is unstable in solution and therefore a new solution was prepared just prior to each injection. From the day of implantation, mice received twice daily an intraperitoneal injection of NaHS until 28 days after implantation. One group of mice ($n = 6$) received a low dose of NaHS (25 μ mol/kg), the other group ($n = 6$) received a high dose of NaHS (50 μ mol/kg), and mice receiving saline injections served as a control group ($n = 6$).

Dynamic Inhaled Gas Test (DIGT)

To closely follow the vascularization process *in vivo*, DIGT measurements were performed on days 3, 7, 21, 35, 49 and 63 after implantation on each animal ($n = 6$ per group). For the DIGT measurements each mouse was anesthetized by 2–3% of isoflurane (Piramel Healthcare, Morpeth, United Kingdom) while breathing 760 mmHg oxygen. When the animals were under full anesthesia the gas was changed to 152 mmHg oxygen and isoflurane level was reduced to 1.5%. The optical monitor was then placed on the skin directly above the implanted device. Following 100 baseline lifetime measurements (spaced by 4.25 s for a total of 425 s), the inhaled gas was switched back to 760 mmHg oxygen. It

is expected that the tissue PO_2 will rise and fall as the inhaled PO_2 is increased and decreased, respectively. Accordingly, once the inhaled gas is returned to 760 mmHg, lifetime values should reach a new plateau, where the time to plateau is an indication of the oxygen transport between the blood, tissue and OSTs. Once the plateau was reached, animals were taken off of anesthesia and returned to their cages. The time to plateau is calculated using custom MATLAB code (MathWorks, Natick, MA, USA) and reported here as *Risetime* (in minutes).

Vessel Morphology

The subcutaneous devices were removed on day 63 after implantation. OSTs were removed from the devices and devices were cut into two pieces; one half of the scaffold was processed for the histological analysis whereas the other half was used for the quantification of vessels by PCR (described below). For histology, the scaffolds were fixated in 2% paraformaldehyde and processed for paraffin embedding. Sections were stained with an overnight incubation of CD31 (1:200; R&D Systems, Abingdon, United Kingdom) after 15 min incubation at 100°C for antigen retrieval (10 mM citrate buffer, pH 6.0) and a subsequent blocking step with 5% donkey serum (Sigma-Aldrich, Zwijndrecht, The Netherlands). The secondary donkey anti-goat alkaline phosphatase conjugated antibody (1:100; Abcam, Cambridge, United Kingdom) was applied for 45 min. Alkaline phosphatase activity was demonstrated by incubating for 10 min with SIGMAFAST™ Fast Red (Sigma-Aldrich, Zwijndrecht, The Netherlands). A short incubation with hematoxylin was used as counterstain. All stained sections were scanned with

the microscope scanner Hamamatsu Nanozoomer (Hamamatsu, Almere, The Netherlands). Scans were analyzed using Aperio ImageScope (Leica Microsystems B.V., Rijswijk, The Netherlands). The number of CD31-positive structures was normalized by the measured scaffold area (mm^2). The fold change was calculated relative to the control.

Vascularization Quantification

To quantify the amount of vessels in the scaffolds, half of the scaffold at day 63 was processed for real-time reverse transcription polymerase chain reaction (RT-PCR) for the vascularization marker CD31. RNA was isolated using Trizol according to the manufacturer's protocol (Invitrogen, Fisher Scientific, Landsmeer, The Netherlands). The RNA concentration was determined using a NanoDrop 1000 spectrophotometer (NanoDrop products, Wilmington, DE, USA). cDNA was reverse transcribed using a SuperScript[®] III Reverse Transcriptase kit according to the instructions of the manufacturer (Life Technologies, USA). RT-PCR was conducted using ViiA[™] Real Time PCR system (Life technologies, Carlsbad, CA, USA) with a primer and probe set (TaqMan Gene Expression Assays, Thermo Fisher Scientific, USA) for CD31 (Mm01242576_m1; Thermo Fisher Scientific, Waltham, MA, USA) and qPCR Mastermix Plus (Eurogentec, Seraing, Belgium). Reactions were performed at 50°C for 2 min, 95°C for 10 min, 95°C for 15 s and 60°C for 60 s repeating in these last two steps for 40 cycles. Delta Ct values were calculated and normalized against the expression of the housekeeping gene GAPDH (Mm99999915_g1; Thermo Fisher Scientific, Waltham, MA, USA). Delta Ct values were used to calculate the fold change compared with gene expression of the control mice.

Statistics

Statistical analysis was carried out in GraphPad Prism (version 7.0d; GraphPad Software, Inc., San Diego, CA, USA). A Shapiro–Wilk normality test was performed to test the data for normality. A Kruskal–Wallis test with Dunn's multiple comparison was performed to study the statistically significant differences for nonparametric distributions. One-way ANOVA with a Tukey post-hoc was performed for parametrically distributed data. p -values <0.05 were considered significant. The data are presented in mean \pm standard deviation in case of parametric distribution and median \pm interquartile range in case of nonparametric distribution.

Results

OST Calibration and DIGT

Prior to implantation, each OST (Fig. 1B) undergoes a gas calibration inside a glass chamber. In this calibration gases with different oxygen levels are inserted into the chamber in order. Fig. 2A shows a calibration process during which the gas mixtures were cycled three times. With each gas

exchange, the corresponding τ is recorded as the mean value of the subsequent plateau. Lifetime values at each oxygen concentration across all three cycles show low variation (standard deviation $< 0.08 \mu\text{s}$). This result demonstrates the repeatability and reliability of oxygen measurements using OST. Following the calibrations, OSTs were inserted into devices, which were implanted as described above. Fig. 2B shows an example of the calculated PO_2 values during a DIGT test. This curve demonstrates an increase in PO_2 levels as reported by the OSTs.

Animal Study

Animals received injections of NaHS (low and high-dosage groups of 25 $\mu\text{mol/kg}$ and 50 $\mu\text{mol/kg}$) and saline (control group) as described above. Injections occurred twice daily for the first 4 weeks (day 28) followed by another 5 weeks of no injections (up to day 63). The follow-up period of 5 weeks with no injections (day 28 to day 63) aims to provide necessary time for device vascularization to complete. The DIGT was performed on all animals ($n = 6$ per group) on days 3, 7, 21, 35, 49, and 63. Fig. 3 (A–C) shows the *Risetime* values calculated from the DIGT measurements on all animals. Statistical differences in lifetimes values were not observed either for each treatment condition across all days, or between treatment conditions on each day. Similarly, DIGT plateau oxygen pressures do not show statistical differences or trends between different conditions or at different timepoints (Fig. 3 (D–F)). These observations indicate vascular perfusion of implants was not affected by administration of the pro-angiogenic H_2S . Fig. 4 shows the histological and gene expression evaluations performed on the explanted devices (explantation on day 63). Surprisingly, statistically different values were observed for the expression of the endothelial cell marker CD31 between treatment groups (Fig. 4D). This may indicate that treatment with a low dose of H_2S can possibly down-regulate the gene expression of CD31 (fold change of 0.57 ± 0.02) compared with the control group and the high-dose group. In addition, histological analysis of CD31 expression shows a similar trend at the protein level (Fig. 4E). Here, CD31-positive vessels were counted in each sample. While the control mice had a mean vessel area density of 40.5 ± 7.5 blood vessels per mm^2 of scaffold, both the low and high treatment groups showed significantly decreased values of 15.0 ± 2 and 18.7 ± 8.3 blood vessels per mm^2 of scaffold, respectively. These results indicate that the vascularization inside the devices may have been negatively affected by the H_2S administrations.

Discussion

The success of subcutaneously implanted cell therapy devices depends on the ability to transfer nutrients and oxygen to implanted cells. It is shown that implantation of such devices can trigger a series of host reactions at the implantation site, such as chronic inflammatory response, granulation

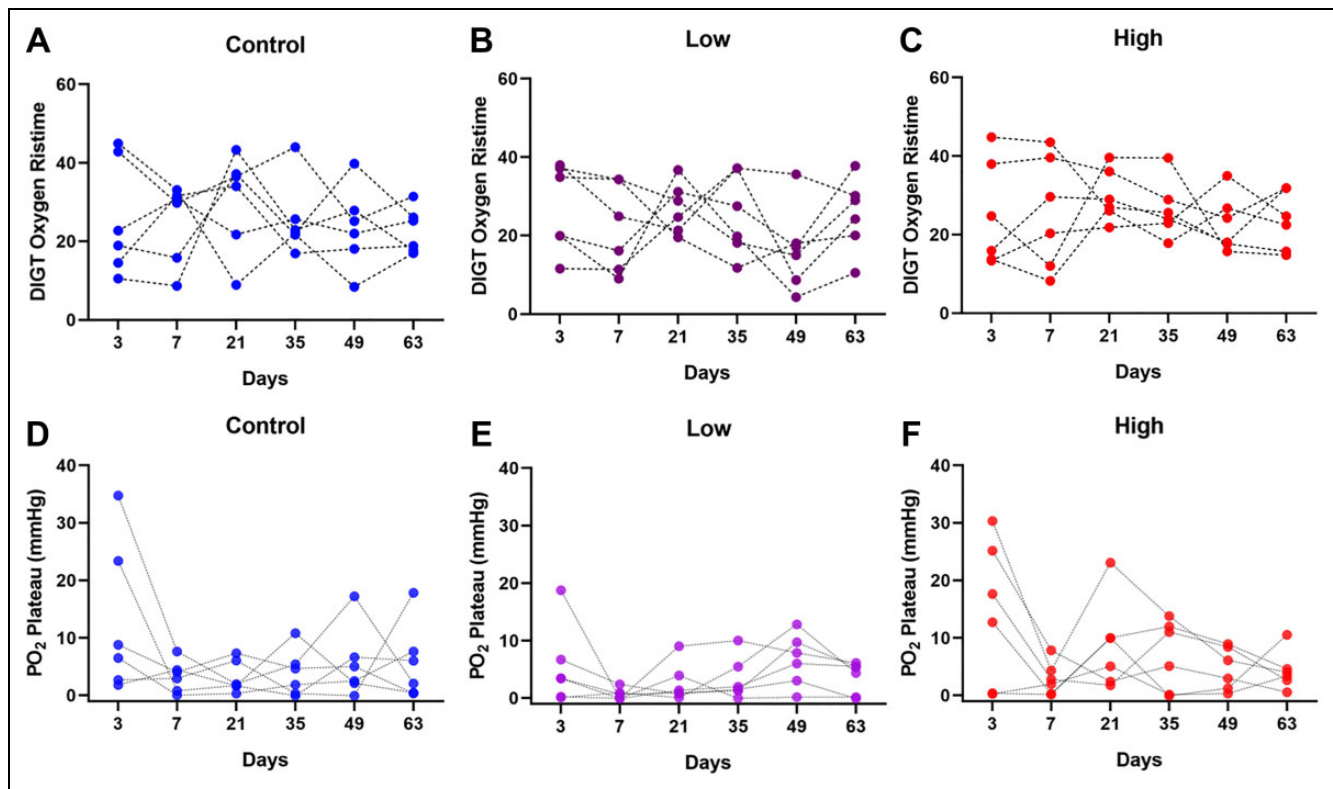


Figure 3. (A–C) DIGT Oxygen Risetime (minutes) and (D–F) PO₂ plateau value (mmHg) at the end of each DIGT experiment, measured for three groups: control (saline), low (25 $\mu\text{mol/kg}$ body weight) and high (50 $\mu\text{mol/kg}$ body weight) NaHS dosages ($n = 6$ per group). All groups underwent twice daily injections for the first 28 days followed by 35 days without injections (day 28 to 63). No statistical differences in Risetime or PO₂ plateau values were detected between groups.

tissue development, foreign body reaction, and fibrosis and fibrous capsule development^{31–36}. The foreign body response often occurs in the first 3 weeks after implantation; after which, wound healing may proceed accompanied with neovascularization of the device³⁶. Invariably, this foreign body reaction can cause formation of diffusional barriers that result in lower availability of nutrients and, importantly, oxygen within the implanted devices. This low availability can result in reduced functionality of the cells and formation of hypoxic conditions, which ultimately can lead to cell death and device failure³⁷. It is therefore necessary to ensure the availability of oxygen and nutrients as delivered by a perfused vasculature. For such vascularization purposes, porous three-dimensional biomaterials have been used as subcutaneous medical devices in the field of tissue engineering^{22,23,26,38}. The pore structure of these biomaterials allows blood vessel infiltration and thereby reduction of diffusional distances and barriers between the neovasculature and the cells. In this study we explore the rate of vascularization and oxygen availability inside porous PDLLCL devices developed by our group^{26,39}. These PDLLCL devices have already shown success in preserving functionality of pancreatic islet cells after subcutaneous implantation, which resulted in achieving normoglycemia in type 1 diabetic animals^{26,39}.

In these previous studies we implanted the devices several weeks before islet transplantation to allow dampening of the foreign body response and ingrowth of blood vessels. When islets were transplanted into these devices, the vascularization supports functional islet survival in the period between transplantation and islet revascularization. However, further improving the vascularization of this device will lead to faster induction of normoglycemia with lower numbers of islets making islet transplantation available for a larger number of type 1 diabetic patients.

H₂S has previously been shown to stimulate endothelial proliferation and migration as well as the development of a new vasculature within Matrigel constructs implanted subcutaneously²⁹. Our results from the non-invasive optical measurements to assess device perfusion *in vivo* showed no significant differences between the control and H₂S-administered groups over the 63-day period of the study. Interestingly, histological and gene expression analysis indicate that H₂S administration may have resulted in lowered formation of neovasculature, an observation not reflected in oxygen dynamics between treatments groups and across days. This suggests that any differences in the extent of vascularization may not be large enough to elicit observable changes in oxygen transport dynamics. The vascular

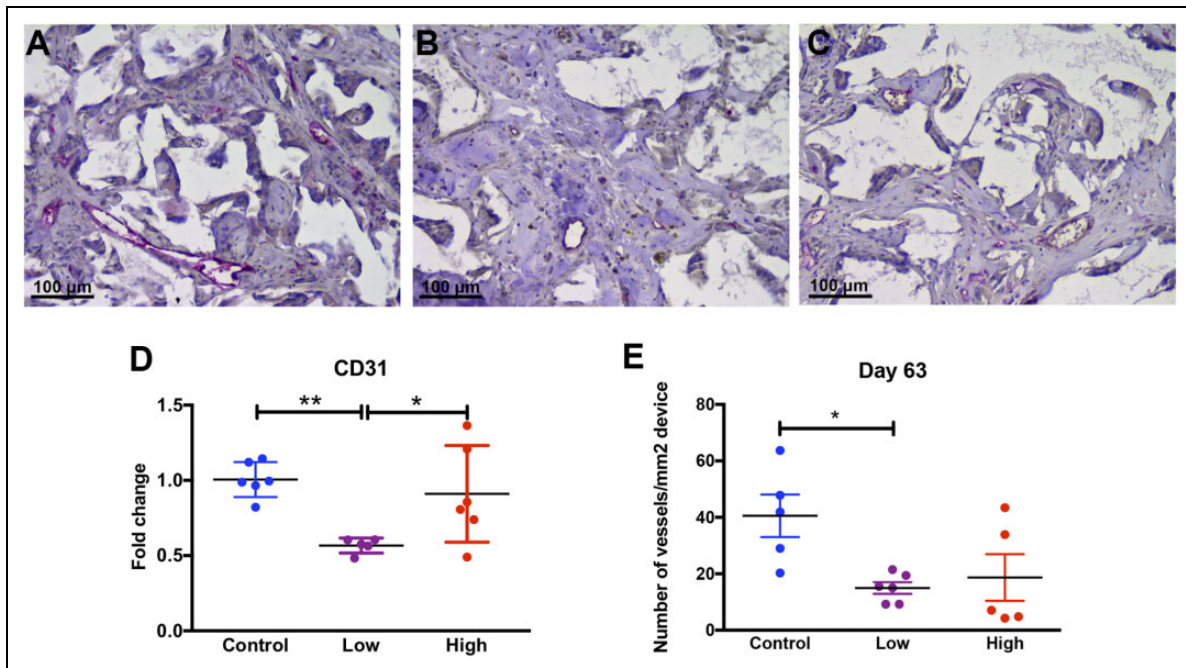


Figure 4. Histological analysis of blood vessels after 63 days of implantation. Blood vessels in the control (A), low H₂S dosage (B), and high H₂S dosage (C) treated groups were stained by using the endothelial cell marker CD31 (pink color). (D) Gene expression of the endothelial cell marker CD31 after 63 days of implantation and (E) the number of vessels per area (mm²) in each device was measured. Data is plotted as mean with the standard error of mean. Statistical analysis was carried out using a one-way ANOVA with a Tukey post-hoc test, $p < 0.05$ (*) and $p < 0.001$ (**).

density as quantified with histology and CD31 expression does not necessarily have to correlate with the DIGT signal, as vascular density does not necessarily reflect the perfusion of the device. For example, consider a cross-sectional view of an oxygen-sensitive rod and its surrounding porous device and tissue. There is a no-flux condition at the tube surface (oxygen is not consumed by the dye) and PO₂ dynamics reported by the tubes are dependent upon (1) diffusional properties of the tissue and device, which do not change at the time scale of a DIGT, and (2) the net rate of transport of oxygen from the vasculature into the device or tissue. These changes are rapid, and depend on PO₂ within the vasculature and blood velocity within them. All things being equal, the primary determinants of DIGT dynamics are total available perfused vessel area, partial pressure of oxygen in the local microvasculature, and tissue or device diffusional properties. We can reliably assume that as vessels invade the device, the system will take less time to reach a new steady state. Accordingly, we anticipate *Risetime* would decrease with increased vessel density and perfusion within the device. In this study, as shown in Fig. 2B for day 3, the PO₂ values rise approximately up to 20 mmHg during the DIGT. These oxygen measurements are exclusive to the surface of OSTs and do not directly measure oxygen partial pressure elsewhere in the device. The observed values are different from what our group has previously reported for DIGT experiments wherein alginate microcapsules containing oxygen-

sensitive microparticles were implanted subcutaneously in Sprague-Dawley rats³⁰. PO₂ levels changed from 45 to 120 mmHg during a day-9 DIGT, at a rate approximately twice that of the present study. These differences indicate that spherical alginate capsules may make for a better environment for delivering oxygen as compared to the investigated device.

In addition to slow dynamics, DIGT experiments reveal low levels of oxygenation within devices measured at the surface of the inserted OSTs. Importantly, our experiment was designed to include six mice per condition, a number estimated to be sufficient when we analyzed perfusion data (total Hb) in the Cai et al. paper. However, DIGT data indicate that six mice is not nearly enough to achieve statistical power at a 95% level of confidence. A Monte Carlo simulation based on observed mean and standard deviations in PO₂ concludes that as many as 20 times more mice would be required. Clearly any H₂S effects are small, and any detectable statistical significance will not translate to benefits to islet transplantation.

Further, our results indicate that the potentiation of vasculature growth and increased perfusion by administration of H₂S in Matrigel²⁹ is not observed for the PDLLCL devices. A previous study by Cai et al. (2007) showed improved angiogenesis in a Matrigel plug after 7 days of intraperitoneal injections of NaHS²⁹. We treated our mice for 28 days with NaHS, indicating that long-term treatment with H₂S

might not significantly affect the vascularization. Further, Dufton et al.⁴⁰ suggest that the administration of hydrogen sulfide using NaHS can result in an increased inflammatory response and triggering of TNF- α formation. Such inflammatory response caused by the injections during the first 4 weeks of implantation, which is also accompanied by foreign body response, may then result in hampering the reported pro-angiogenic characteristics of the H₂S.

In summary, we show that the subcutaneously implanted PDLLCL devices become vascularized in such a way that is resistant to improved vascularization via H₂S treatment. However, we have used similar devices in pancreatic islet implantation studies showing maintenance of islet function with partial or total reversal of chronic hyperglycemia. This may indicate that material properties of the PDLLCL, device geometry, and pore characteristics play roles in governing vascularization, a hypothesis supported by our previous work and consistent with current thinking in the area of biomaterials. Importantly, because our technology can sustain islet function without the need for pharmaceutical factors, it may be categorized as a drug-independent device, which is preferable as a medical product for regulatory agencies.

Acknowledgments

The authors would like to thank Dr. Shiri Li and Antonio Flores for performing animal surgeries and assistance. The authors would like to also thank Michael Alexander for arranging animal procedures.

Ethical Approval

This study was performed with the approval of Institutional Animal Care and Use Committee (IACUC # 2008-2850) at University of California Irvine.

Statement of Human and Animal Rights

This article does not contain any studies with human. All animal subjects were treated and tested with maximum care under the supervision of Institutional Animal Care and Use Committee (IACUC # 2008-2850) at University of California Irvine.

Statement of Informed Consent

There are no human subjects in this article and informed consent is not applicable.


Declaration of Conflicting Interests


The author(s) declared no potential conflicts of interest with respect to the research, authorship, and/or publication of this article.

Funding

The author(s) disclosed receipt of the following financial support for the research, authorship, and/or publication of this article: The authors acknowledge generous funding from Juvenile Diabetes Research Foundation (3-SRA-2016-255-S-B) for supporting this work.

ORCID iDs

Avid Najdahmadi  <https://orcid.org/0000-0001-5702-3922>

Jonathan R.T. Lakey  <https://orcid.org/0000-0001-8553-4287>

References

1. Langer RS, Vacanti JP. Tissue engineering: the challenges ahead. *Sci Am*. 1999;280(4):86–89.
2. Hoffman AS. Hydrogels for biomedical applications. *Adv Drug Deliv Rev*. 2012;64:18–23.
3. Shapiro AM, Lakey JR, Ryan EA, Korbitt GS, Toth E, Warnock GL, Kneteman NM, Rajotte RV. Islet transplantation in seven patients with type 1 diabetes mellitus using a glucocorticoid-free immunosuppressive regimen. *N Engl J Med*. 2000;343(4):230–238.
4. Yoon J-W, Jun H-S. Autoimmune destruction of pancreatic B cells. *Am J Ther*. 2005;12(6):580–591.
5. Gillard P, Keymeulen B, Mathieu C. Beta-cell transplantation in type 1 diabetic patients: a work in progress to cure. *Verh K Acad Geneesk Belg*. 2010;72(1-2):71–98.
6. The Diabetes Control and Complications Trial/Epidemiology of Diabetes Interventions and Complications (DCCT/EDIC) Study Research Group. Intensive diabetes treatment and cardiovascular disease in patients with type 1 diabetes. *N Engl J Med*. 2005;353(25):2643–2653.
7. Diabetes Control and Complications Trial/Epidemiology of Diabetes Interventions and Complications Research Group; Lachin JM, Genuth S, Cleary P, Davis MD, Nathan DM. Retinopathy and nephropathy in patients with type 1 diabetes four years after a trial of intensive therapy. *N Engl J Med*. 2000;342(6):381–389.
8. Dholakia S, Oskrochi Y, Easton G, Papalois V. Advances in pancreas transplantation. *J R Soc Med*. 2016;109(4):141–146.
9. Hering BJ. Achieving and maintaining insulin independence in human islet transplant recipients. *Transplantation*. 2005;79(10):1296–1297.
10. Froud T, Ricordi C, Baidal DA, Hafiz MM, Ponte G, Cure P, Pileggi A, Poggioli R, Ichii H, Khan A, Ferreira JV, et al. Islet transplantation in type 1 diabetes mellitus using cultured islets and steroid-free immunosuppression: Miami experience. *Am J Transplant*. 2005;5(8):2037–2046.
11. Juang J-H, Bonner-Weir S, Ogawa Y, Vacanti JP, Weir GC. Outcome of subcutaneous islet transplantation improved by polymer device. *Transplantation*. 1996;61(11):1557–1561.
12. Pileggi A, Molano RD, Ricordi C, Zahr E, Collins J, Valdes R, Inverardi L. Reversal of diabetes by pancreatic islet transplantation into a subcutaneous, neovascularized device. *Transplantation*. 2006;81(9):1318–1324.
13. de Vos P, Hamel AF, Tatarkiewicz K. Considerations for successful transplantation of encapsulated pancreatic islets. *Diabetologia*. 2002;45(2):159–173.
14. Najdahmadi A, Lakey JRT, Botvinick E. Structural characteristics and diffusion coefficient of alginate hydrogels used for cell based drug delivery. *MRS Adv*. 2018;3(40):2399–2408.
15. Najdahmadi A, Lakey JR, Botvinick E. Diffusion coefficient of alginate microcapsules used in pancreatic islet transplantation, a method to cure type 1 diabetes. *Nanoscale Imaging, Sensing, and Actuation for Biomedical Applications XV*. San Francisco (CA): International Society of Optics and Photonics; 2018.

16. de Vos P, Spasojevic M, Faas MM. Treatment of diabetes with encapsulated islets. *Adv Exp Med Biol.* 2010;670:38–53.
17. Smink AM, de Haan BJ, Lakey JRT, de Vos P. Polymer scaffolds for pancreatic islet transplantation - Progress and challenges. *Am J Transplant.* 2018;18(9):2113–2119.
18. Sakata N, Aoki T, Yoshimatsu G, Tsuchiya H, Hata T, Katayose Y, Egawa S, Unno M. Strategy for clinical setting in intramuscular and subcutaneous islet transplantation. *Diabetes Metab Res Rev.* 2014;30(1):1–10.
19. Pepper AR, Pawlick R, Gala-Lopez B, MacGillivray A, Mazzuca DM, White DJ, Toleikis PM, Shapiro AM. Diabetes is reversed in a murine model by marginal mass syngeneic islet transplantation using a subcutaneous cell pouch device. *Transplantation.* 2015;99(11):2294–2300.
20. Shimizu S, Eguchi Y, Kamiike W, Itoh Y, Hasegawa J, Yamabe K, Otsuki Y, Matsuda H, Tsujimoto Y. Induction of apoptosis as well as necrosis by hypoxia and predominant prevention of apoptosis by Bcl-2 and Bcl-XL. *Cancer Res.* 1996;56(9):2161–2166.
21. Dufour JM, Rajotte RV, Zimmerman M, Rezanian A, Kin T, Dixon DE, Korbitt GS. Development of an ectopic site for islet transplantation, using biodegradable scaffolds. *Tissue Eng.* 2005;11(9–10):1323–1331.
22. Pedraza E, Brady A-C, Fraker CA, Molano RD, Sukert S, Berman DM, Kenyon NS, Pileggi A, Ricordi C, Stabler CL. Macroporous three-dimensional PDMS scaffolds for extrahepatic islet transplantation. *Cell Transplant.* 2013;22(7):1123–1135.
23. Ratner BD. A pore way to heal and regenerate: 21st century thinking on biocompatibility. *Regen Biomater.* 2016;3(2):107–110.
24. Phelps EA, Templeman KL, Thulé PM, García AJ. Engineered VEGF-releasing PEG–MAL hydrogel for pancreatic islet vascularization. *Drug Deliv Transl Res.* 2013;5(2):125–136.
25. Lovett M, Lee K, Edwards A, Kaplan DL. Vascularization strategies for tissue engineering. *Tissue Eng Part B Rev.* 2009;15(3):353–370.
26. Smink AM, Li S, Hertsig DT, de Haan BJ, Schwab L, van Apeldoorn AA, de Koning E, Faas MM, Lakey JR, de Vos P. The efficacy of a prevascularized, retrievable poly(D, L,-lactide-co-ε-caprolactone) subcutaneous scaffold as transplantation site for pancreatic islets. *Transplantation.* 2017;101(4):e112–e119.
27. Abe K, Kimura H. The possible role of hydrogen sulfide as an endogenous neuromodulator. *J Neurosci.* 1996;16(3):1066–1071.
28. Kanagy NL, Szabo C, Papapetropoulos A. Vascular biology of hydrogen sulfide. *Am J Physiol Cell Physiol.* 2017;312(5):C537–C549.
29. Cai W-J, Wang M-J, Moore PK, Jin H-M, Yao T, Zhu Y-C. The novel proangiogenic effect of hydrogen sulfide is dependent on Akt phosphorylation. *Cardiovasc Res.* 2007;76(1):29–40.
30. Weidling J, Sameni S, Lakey JRT, Botvinick E. Method measuring oxygen tension and transport within subcutaneous devices. *J Biomed Opt.* 2014;19(8):087006.
31. Luttkhuizen DT, Harmsen MC, Van Luyn MJA. Cellular and molecular dynamics in the foreign body reaction. *Tissue Eng.* 2006;12(7):1955–1970.
32. Wynn TA. Common and unique mechanisms regulate fibrosis in various fibroproliferative diseases. *J Clin Invest.* 2007;117(3):524–529.
33. Morais JM, Papadimitrakopoulos F, Burgess DJ. Biomaterials/tissue interactions: possible solutions to overcome foreign body response. *AAPS J.* 2010;12(2):188–196.
34. Campos PP, Andrade SP, Moro L, Ferreira MAND, Vasconcelos AC. Cellular proliferation, differentiation and apoptosis in polyether-polyurethane sponge implant model in mice. *Histol Histopathol.* 2006;21(12):1263–1270.
35. Mendes JB, Rocha MA, Araújo FA, Moura SAL, Ferreira MAND, Andrade SP. Differential effects of rolipram on chronic subcutaneous inflammatory angiogenesis and on peritoneal adhesion in mice. *Microvasc Res.* 2009;78(3):265–271.
36. Anderson JM, Rodriguez A, Chang DT. Foreign body reaction to biomaterials. *Semin Immunol.* 2008;20(2):86–100.
37. Michiels C. Physiological and pathological responses to hypoxia. *Am J Pathol.* 2004;164(6):1875–1882.
38. Xiao X, Wang W, Liu D, Zhang H, Gao P, Geng L, Yuan Y, Lu J, Wang Z. The promotion of angiogenesis induced by three-dimensional porous beta-tricalcium phosphate scaffold with different interconnection sizes via activation of PI3K/Akt pathways. *Sci Rep.* 2015;5:9409.
39. Smink AM, Hertsig DT, Schwab L, van Apeldoorn AA, de Koning E, Faas MM, de Haan BJ, de Vos P. A retrievable, efficacious polymeric scaffold for subcutaneous transplantation of rat pancreatic islets. *Ann Surg.* 2017;266(1):149–157.
40. Dufton N, Natividad J, Verdu EF, Wallace JL. Hydrogen sulfide and resolution of acute inflammation: a comparative study utilizing a novel fluorescent probe. *Sci Rep.* 2012;2:499.